Research Article | Vol. 9, No. 11 / 1 November 2019 / Optical Materials Express 4318
Optical Materials EXPRESS

UV to NIR optical properties of IP-Dip, IP-L, and IP-S after two-photon polymerization determined by spectroscopic ellipsometry

Y. Li,[1,*] S. Park,[1] M. McLamb,[1] M. Lata,[1] S. Schöche,[2] D. Childers,[3] I. D. Aggarwal,[1] M. K. Poutous,[1] G. Boreman,[1] and T. Hofmann[1,4]

[1]Department of Physics and Optical Science, University of North Carolina at Charlotte, 9201 University City Blvd., Charlotte, NC 28223, USA
[2]J. A. Woollam Co., Inc., 645 M Street, Lincoln, NE 68508, USA
[3]USCONEC, 1138 25th Street Southeast, Hickory, NC 28602, USA
[4]THz Materials Analysis Center, Department of Physics, Chemistry, and Biology (IFM), Linköping University, SE 581 83 Linköping, Sweden
[*]yli91@uncc.edu

Abstract: The polymers IP-Dip, IP-L, and IP-S are among the most commonly used photo-resists employed for the rapid prototyping of optical components using two-photon polymerization. Despite the widespread use of these polymers, measured data on their optical properties is scarce. Recently, the refractive index n of these polymers has been determined in the visible and near-infrared spectral range. However, the accurate optical properties including extinction coefficient κ in the ultraviolet spectral range have not been reported yet. Here we report on accurate, ellipsometric measurements of the complex dielectric functions of two-photon polymerized IP-Dip, IP-L, and IP-S in the spectral range from 210 nm to 1500 nm. Model dielectric functions composed of oscillators with Lorentz, Gaussian, and Tauc-Lorentz broadenings are presented for all investigated polymers.

1. Introduction

Three-dimensional direct laser writing (3D-DLW) based on two-photon polymerization has enabled the fabrication of optical components composed of sub-wavelength-sized elements, forming virtually arbitrary architectures in free space [1]. First demonstrated in 2004 for the synthesis of infrared photonic crystals [2], two-photon polymerization is now widely employed for the synthesis of three-dimensional structures with a spatial resolution ranging from nm- to μm-scales [3–5]. Contemporary applications of this technique have enabled the fabrication of complex optical components [6–8]. Recently, 3D-DLW has been successfully employed for the synthesis of metamaterials [9–12]. The optical components and materials fabricated using 3D-DLW cover a very wide spectral range from the ultraviolet (UV) through the visible (VIS) to the near-infrared (NIR) [13–17]. In addition, 3D-DLW-based fabrication of micro-optical elements with functional coatings and the manufacturing of metasurfaces have attracted much attention [8,18–21].

Despite the demonstration of optical components using 3D-DLW-based fabrication techniques, reports on the optical properties of 3D-DLW-compatible polymers are still scarce [22–24]. This lack of accurate knowledge of the optical constants of 3D-DLW-compatible polymers impedes further advances in the design and optimization of novel metamaterials and optical components fabricated using 3D-DLW-based approaches.

We have recently reported on the infrared complex dielectric functions of two commercially available and frequently employed 3D-DLW-compatible polymers IP-Dip and IP-L (Nanoscribe

#374318 https://doi.org/10.1364/OME.9.004318
Journal © 2019 Received 31 Jul 2019; revised 26 Sep 2019; accepted 29 Sep 2019; published 15 Oct 2019

Optical Materials EXPRESS

GmbH) determined using spectroscopic ellipsometry in the infrared spectral range from 1.67 μm to 40 μm [23]. T. Gissibl *et al.* extended the spectral range towards the visible spectral region from 400 nm to 900 nm by determining the refractive indices n of the UV-cured polymers including IP-Dip, IP-L, and IP-S using refractometry [22]. Recently, S. Dottermusch *et al.* have further explored the exposure-dependent refractive index of IP-Dip in the spectral range from 400 nm to 1550 nm [24]. An index difference Δn of up to 0.01 between single-photon polymerized (UV-cured) and two-photon polymerized IP-Dip was found. However, these recent reports focused exclusively on the transparent region of single-photon polymerized polymers [22] and the extinction coefficient κ has only been reported for single-photon polymerized IP-Dip so far [24]. The complex refractive index of two-photon polymerized IP-Dip, IP-L, and IP-S in the spectral range from 210 nm to 400 nm has not been reported yet. Furthermore, parameterized dielectric function models are currently not available for these two-photon polymerized materials in the spectral range from 210 nm to 1500 nm.

In this paper, we report on the complex dielectric functions of two-photon polymerized IP-Dip, IP-L, and IP-S in the UV–VIS –NIR sepctral range (210 nm to 1500 nm) determined using spectroscopic ellipsometry. A parameterized dielectric function model composed of a sum of oscillators with Gaussian, Lorentz, and Tauc-Lorentz broadenings is used to accurately describe the optical response of these polymers in the measured spectral range. A good agreement is found between the refractive index obtained here and the previous reports which focused on the transparent spectral range from 400 nm to 900 nm [22,24]. Common for all investigated polymers is the strong absorption for wavelenghts below 400 nm, but the number, strength, amplitude, and broadening of the observed absorption bands differ substantially between two-photon polymerized IP-Dip, IP-L, and IP-S.

2. Experiment

2.1. Sample preparation

Here the focus is on three commonly used, 3D-DLW-compatible polymers, which are commercially available as IP-Dip, IP-L, and IP-S (Nanoscribe, GmbH). The difference in viscosity between IP-Dip, IP-L, and IP-S allows the fabrication of structures with a wide range of critical dimensions in the nm to the μm range [13,25,26]. For each polymer, two samples in the shape of rectangular cuboids with a 100 μm $\times$ 100 μm base and two different heights were fabricated on Si substrates using a commercially available 3D-DLW system (Photonic Professional GT, Nanoscribe, GmbH). The nominal heights for the samples ranged between 2000 nm to 4500 nm. Prior to the 3D-DLW fabrication, the Si substrates were rinsed with Acetone and Methanol. All samples were fabricated in a single 3D-DLW fabrication step. A 25$\times$ objective was employed. This allows the fabrication of the rectangular cuboids by steering the laser beam with the galvanometer scanner of the 3D-DLW system. This approach dispenses with the need for any mechanical translation of the sample stage and thereby avoids possible stitching and over-exposure errors that may be induced by a mechanical translation of the sample [27]. A laser power and scan speed of 90% and 20000 μm/s (nominal DeScribe settings, Nanoscribe GmbH), respectively, were used to minimize fabrication time while preventing over-exposure. After the fabrication, any unpolymerized monomer was removed by immersing the samples in propylene glycol monomethyl ether acetate (PGMEA, Baker 220) for 20 min. Subsequently, the samples were immersed in 99.99% isopropyl alcohol for 2 min. Finally, the remaining isopropyl alcohol was evaporated at room temperature.

2.2. Data acquisition and analysis

The IP-Dip, IP-L, and IP-S samples were investigated using a commercial spectroscopic ellipsometer (RC2, J.A. Woollam Company Inc.) in the spectral range from 210 nm to 1500 nm at a fixed angle of incidence of Φ_a=65°. The ellipsometer operates in a rotating compensator

Optical Materials EXPRESS

configuration and is capable of measuring all 16 normalized, real-valued Mueller matrix elements M_{ij}/M_{11}, which connect the Stokes parameters of the probe beam before and after interaction with the sample [28]. The instrument is equipped with focusing optics and allows accurate ellipsometric data acquisition on a very small sample area with the size of 25×60 μm^2 at a single angle of incidence. For the ellipsometric measurements, the samples were aligned such that the entire probe beam fitted within the base surface area of the cuboid-shaped samples. This approach simplified the data analysis during which the samples were treated as homogeneous thin films. Two ellipsometric data sets were obtained for each polymer, one data set for each cuboid with a given height. These data sets were analyzed simultaneously. This well known multi-sample analysis approach reduces possible parameter correlation, which might arise from the ellipsometric measurements restricted instrumentally to a single angle of incidence [29].

The experimental and best-model Mueller matrix spectra M_{ij}/M_{11} are shown in Figs. 1, 2, and 3 for IP-Dip, IP-L, and IP-S, respectively. As expected, the observed optical responses of the fabricated samples are isotropic, i.e., only the on-diagonal block Mueller matrix elements are non-trivial and the off-diagonal Mueller matrix elements are negligible [30]. The experimental data were analyzed using stratified-layer optical model calculations employing a commercial ellipsometry data analysis software package (WVASE32, J.A. Woollam Co.).

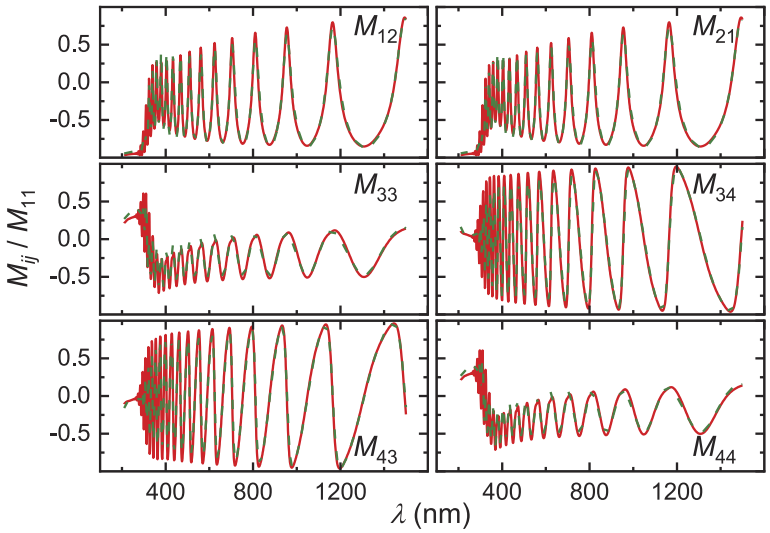

Fig. 1. Experimental (green dashed lines) and best-model calculated (red solid lines) Mueller matrix spectra of the two-photon polymerized IP-Dip sample with a nominal thickness of 2100 nm for the spectral range from 210 nm to 1500 nm. The angle of incidence was $\Phi_a = 65°$. The data for the sample with a nominal thickness of 3500 nm is omitted here for clarity, but shows also excellent agreement between experimental and best-model calculated line shapes.

Stratified layer optical models composed of three layers including Si substrate, SiO_2 layer, and a polymer layer are employed for the analysis of the experimental Mueller matrix spectra. The native SiO_2 layer thickness was determined using ellipsometric data obtained from the Si substrate prior to the sample fabrication. The layer thickness of the native SiO_2 was not further varied during the analysis of the ellipsometric data measured for the IP-Dip, IP-L, and IP-S samples. Standard model dielectric functions were used to account for the optical response of the Si substrate and the SiO_2 layer [29].

The parameterized complex dielectric function of the polymers needs to accurately render the optical response of these materials over a wide spectral range from the NIR to the UV. Dielectric

Optical Materials EXPRESS

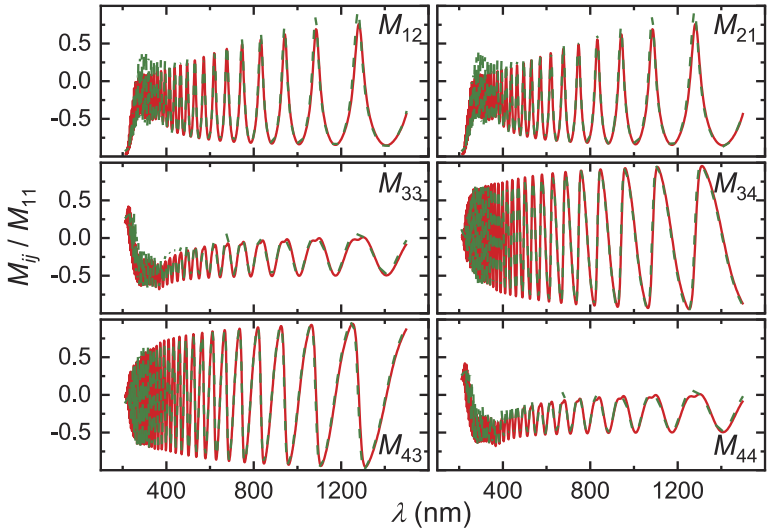

Fig. 2. Experimental (green dashed lines) and best-model calculated (red solid lines) Mueller matrix spectra of the two-photon polymerized IP-L sample with a nominal thickness of 2900 nm for the spectral range from 210 nm to 1500 nm. The angle of incidence was $\Phi_a = 65°$. The data for the sample with a nominal thickness of 4300 nm is omitted here for clarity, but shows also an excellent agreement between experimental and best-model calculated line shapes.

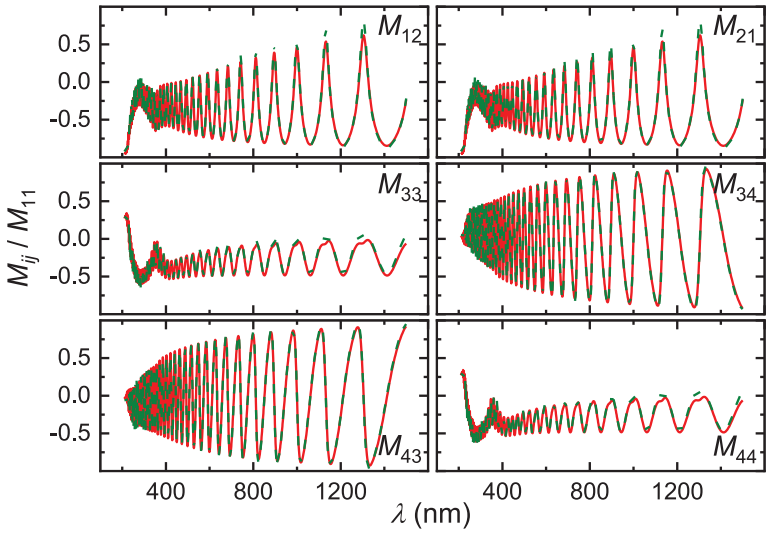

Fig. 3. Experimental (green dashed lines) and best-model calculated (red solid lines) Mueller matrix spectra of the two-photon polymerized IP-S sample with a nominal thickness of 3500 nm for the spectral range from 210 nm to 1500 nm. The angle of incidence was $\Phi_a = 65°$. As for the IP-Dip and IP-L data shown in Figs. 1 and 2, respectively, the data for the sample with a nominal thickness of 4500 nm is omitted here for clarity, but shows also an excellent agreement between the experimental and best-model calculated line shapes.

Optical Materials EXPRESS

function models composed of oscillators with different broadenings have been demonstrated to accurately describe the material dielectric functions throughout the UV, VIS , and IR spectral ranges, while simultaneously ensuring Kramers-Kronig consistency in the determined optical constants [31]. Here, parameterized dielectric functions composed of a combination of oscillators with Gaussian, Lorentz, and Tauc-Lorentz broadenings are used to describe the optical responses of two-photon polymerized IP-Dip, IP-L, and IP-S:

$$\begin{aligned}\varepsilon(E) &= \varepsilon_1(E) + i\varepsilon_2(E)\,, \\ &= \varepsilon_\infty + \frac{A}{E_0^2 - E^2} + \sum^{l} \mathrm{Gau}(A, E_0, \Gamma, E) + \sum^{m} \mathrm{Lor}(A, E_0, \Gamma, E) \\ &\quad + \sum^{n} \mathrm{TL}(A, E_0, \Gamma, E_g, E).\end{aligned} \tag{1}$$

The real and imaginary parts of the complex dielectric function $\varepsilon(E)$ are denoted by $\varepsilon_1(E)$ and $\varepsilon_2(E)$, respectively, as functions of the photon energy E. The functions $\mathrm{Gau}(A, E_0, \Gamma, E)$, $\mathrm{Lor}(A, E_0, \Gamma, E)$, and $\mathrm{TL}(A, E_0, \Gamma, E_g, E)$ represent oscillators with Gaussian, Lorentz, and Tauc-Lorentz broadening, respectively, where A is the oscillator amplitude, Γ the oscillator broadening, and E_0 the oscillator energy. For the Tauc-Lorentz oscillator the Tauc gap E_g denotes the energy at which $\varepsilon_2 = 0$. ε_∞ is a constant offset to $\varepsilon_1(E)$. Higher energy contributions to the dielectric function cause absorptions outside of the measured spectral range, which contribute to the dispersion of $\varepsilon_1(E)$. These contributions are included in the model by a pole, i.e., a Lorentz oscillator with vanishing broadening $A/(E_0^2 - E^2)$.

The imaginary part of the dielectric function $\varepsilon_2(E)$ for the oscillators with Gaussian $\varepsilon_2^{\mathrm{Gau}}(E)$, Lorentz $\varepsilon_2^{\mathrm{Lor}}(E)$, and Tauc-Lorentz $\varepsilon_2^{\mathrm{TL}}(E)$ broadening is given by [31–33]:

$$\varepsilon_2^{\mathrm{Gau}}(E) = Ae^{-\left(\frac{E-E_0}{f\cdot\Gamma}\right)^2} - Ae^{-\left(\frac{E+E_0}{f\cdot\Gamma}\right)^2}, \tag{2}$$

$$\varepsilon_2^{\mathrm{Lor}}(E) = \frac{AE_0\Gamma}{E_0^2 - E^2 - i\Gamma E}\,, \tag{3}$$

$$\varepsilon_2^{\mathrm{TL}}(E) = \begin{cases} \frac{AE_0\Gamma(E-E_g)^2}{(E^2-E_0^2)^2+\Gamma^2E^2}\cdot\frac{1}{E} & E>E_g \\ 0 & E \le E_g\,, \end{cases} \tag{4}$$

where the constant $f = 1/2\sqrt{\ln(2)}$ in Eqn. (2) defines the full width at half maximum for the broadening Γ. The real part $\varepsilon_1(E)$ is obtained by a Kramers-Kronig integration of ε_2(E) given in Eqns. (2)–(4) as part of the data analysis.

During the data analysis of the experimental Mueller matrix data obtained for the IP-Dip, IP-L, and IP-S samples, the relevant model parameters are varied using a Levenberg-Marquardt-based algorithm until the experimental and model calculated data match as close as possible (best-model). The best-model parameters obtained for the oscillator amplitude, energy, and broadening for IP-Dip, IP-L, and IP-S are summarized in Tab. 1. The corresponding optical constants are shown in Figs. 4, 5, and 6, respectively.

Optical Materials EXPRESS

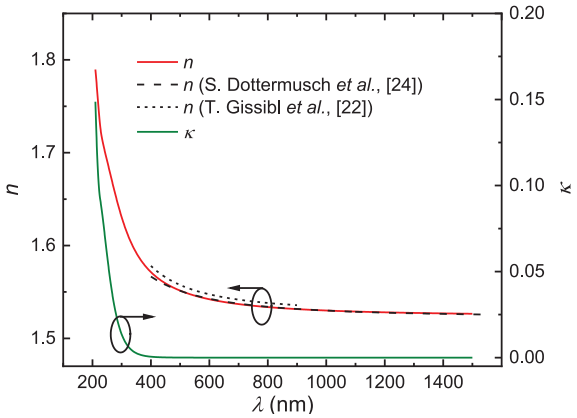

Fig. 4. The best-fit model refractive index n (red solid line) and extinction coefficient κ (green dashed line) for two-photon polymerized IP-Dip in the spectral range from 210 nm to 1500 nm. The spectrum below 400 nm is dominated by absorption bands, which are described by two oscillators with Tauc-Lorentz and Gaussian broadening. The best-model parameters are summarized in Table 1. The refractive index of two-photon polymerized (black dashed line) and single-photon polymerized (black dotted line) IP-Dip reported by S. Dottermusch *et al.* and T. Gissibl *et al.*, respectively, are reproduced for comparison [22,24].

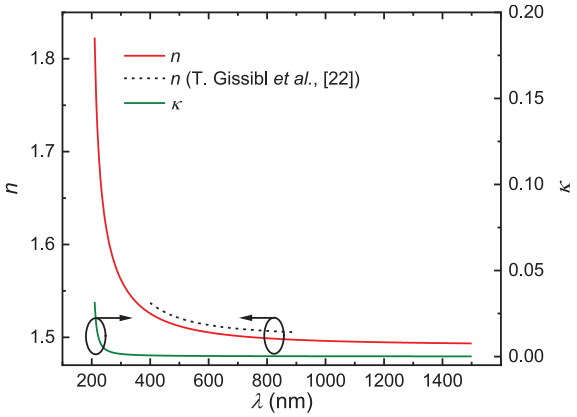

Fig. 5. Same as Fig. 4 but for IP-L. IP-L is characterized by a sharp absorption onset which can be described by a single Lorentz oscillator. The best-model parameters are summarized in Table 1. The refractive index of single-photon polymerized IP-L (black dotted line) reported by T. Gissibl *et al.* is shown for comparison [22].

Table 1. All Polymers best-model oscillator parameters, with errors representing the 90% confidence limits of the model parameters

	Oscillator	A	E_0 (eV)	Γ (eV)	E_g (eV)
IP-Dip	TL	(135.87±4.18) eV	6.34±0.05	3.95±0.70	5.48±0.01
	Gau	0.69±0.13	5.84±0.13	1.98±0.08	—
IP-L	Pole	(70.84±0.68) eV^2	10.43±0.02	—	—
	Lor	0.83±0.03	6.37±0.02	0.12±0.01	—
IP-S	Pole	(65.81±0.50) eV^2	9.82±0.01	—	—
	Lor	1.72±0.09	6.24±0.02	0.17±0.01	—
	Gau	0.01±0.001	3.47±0.01	0.53±0.01	—

Optical Materials EXPRESS

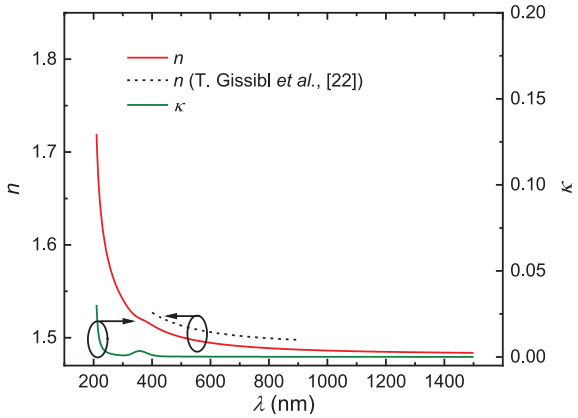

Fig. 6. Same as Fig. 4 but for IP-S, which can be described using two oscillators with Lorentz and Gaussian broadening. The best-model parameters are summarized in Table 1. In addition to the sharp absorption onset below 300 nm, a small absorption band at 358 nm can be observed. The refractive index of single-photon, UV-cured IP-S (black dotted line) reported by T. Gissibl *et al.* is shown for comparison [22].

3. Results and discussion

Figures 1, 2, and 3 show experimental (green dashed lines) and best-model calculated (red solid lines) Mueller matrix spectra obtained in the spectral range from 210 nm to 1500 nm for the two-photon polymerized IP-Dip, IP-L, and IP-S samples, with a nominal thickness of 2100 nm, 2900 nm, and 3500 nm, respectively. The angle of incidence was fixed at $\Phi_a = 65°$ for all measurements. Only the non-trivial Mueller matrix elements expected for isotropic sample responses, M_{12}, M_{21}, M_{33}, M_{34}, M_{34}, and M_{43}, are shown for brevity [30].

An excellent agreement between the experimental and best-model calculated data was found for all polymers. Note that for each polymer two samples with different thicknesses were analyzed simultaneously using a common dielectric function. The effects of the angular spread, caused by the used of focusing optics, are included in the model calculation. The best-model values for the angular spread were approximately 6°, which is typical for the employed ellipsometer equipped with focusing optics.

The Mueller matrix spectra shown in Fig. 1 for the IP-Dip sample are dominated by a Fabry-Pérot interference pattern in the spectral range from 400 nm to 1500 nm, which originates from the plane-parallel interfaces of the polymer. As the wavelength approaches the ultraviolet region below 400 nm, a significant dampening of the interference amplitude can be recognized. This indicates the presence of substantial absorption bands in the spectral range from 210 nm to 400 nm.

A similar optical response can be observed in the Mueller matrix spectra of IP-L and IP-S depicted in Fig. 2 and 3, respectively. However, the positions and amplitudes of the absorption bands are different among the three investigated polymers.

Table 1 summarizes the the best-model fit parameters for the mixed oscillator model dielectric functions of IP-Dip, IP-L, and IP-S, respectively. Accurate rendering of the experimental Mueller matrix data of IP-Dip requires a combination of two oscillators including an oscillator with Tauc-Lorentz and one with Gaussian broadening. In the model dielectric function of IP-L two Lorentz oscillators and one pole were used. For the model dielectric function of IP-S, three oscillators including one pole with two broadening types (Gaussian and Lorentz) were required. The best-fit values for the static dielectric constants ε_∞ of the investigated polymers were comparable. The largest value was found for IP-S with $\varepsilon_\infty = 1.46 \pm 0.01$. The values for

Optical Materials EXPRESS

IP-Dip and IP-L are slightly smaller with $\varepsilon_\infty = 1.43 \pm 0.04$ for IP-Dip and $\varepsilon_\infty = 1.44 \pm 0.01$ for IP-L. The best-model parameters for the thicknesses of the polymer samples are $t_{\text{IP-Dip}} = 2124 \pm 4$ nm, $t_{\text{IP-L}} = 2940 \pm 1$ nm and $t_{\text{IP-S}} = 3582 \pm 4$ nm, which are in good agreement with the nominal values as expected from the 3D-DLW fabrication.

Figures 4, 5, and 6 depict the refractive index n (red solid lines) and extinction coefficient κ (green solid lines) of the best-fit model for IP-Dip, IP-L, and IP-S in the spectral range from 210 nm to 1500 nm, respectively. The refractive index data reported by S. Dottermusch *et al.* for two-photon polymerized (black dashed line) IP-Dip [24] and by T. Gissibl *et al.* for single photon polymerized IP-Dip, IP-L, and IP-S (black dotted lines) [22] are included in Figs. 4–6 for comparison.

An excellent agreement of the refractive index determined using a mixed oscillator model dielectric function here and the refractive index reported in Refs. [24] can be observed for two-photon polymerized IP-Dip (Fig. 4) in the spectral region where the polymer is transparent. As expected, a small difference can be noticed between the refractive index of single-photon polymerized (UV cured) polymers and the corresponding two-photon polymerized IP-Dip, IP-L, and IP-S [22]. For all three investigated polymers, the refractive index of the single-photon polymerized sample is higher than the refractive index of the two-photon polymerized sample. Therefore, optical elements that rely on a small index difference of adjacent polymer layers, like the waveguides suggested by Dottermusch *et al.*, could be realized using all of the investigated polymers [24].

To provide a direct comparison of the optical properties for the investigated polymers, the determined refractive indices n and extinction coefficients κ have been presented together in Fig. 7. Comparing the refractive indices n shown in panel (a) of Fig. 7, one can easily verify that the two-photon polymerized IP-Dip has the highest refractive index among the investigated polymers in the VIS spectral range. The refractive indices of IP-L and IP-S are grouped closely together and are substantially smaller compared to the refractive index of IP-Dip. The wider transparent window of IP-L and IP-S compared to IP-Dip can be immediately observed in Fig. 7(b).

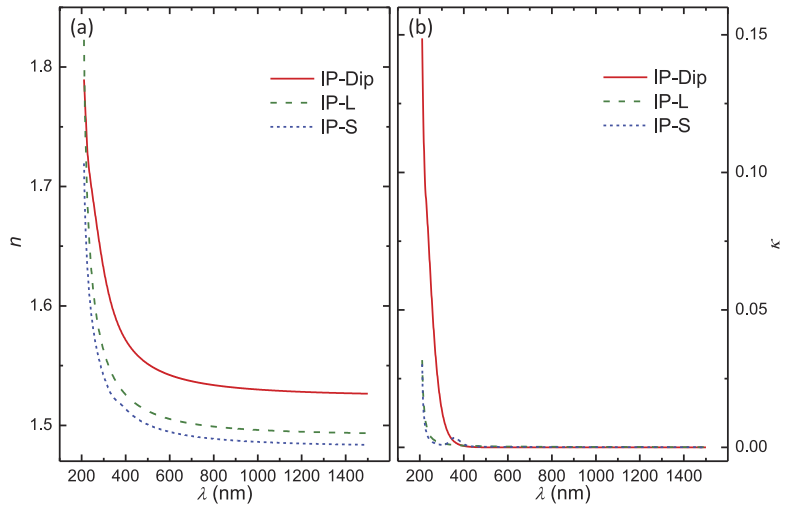

Fig. 7. The best-fit model refractive indices n and extinction coefficients κ for the two-photon polymerized IP-Dip, IP-L, and IP-S are reproduced in panel (a) and (b), respectively, for a direct comparison.

Common for all polymers is also the strong absorption in the UV spectral range. However, while IP-Dip is transparent up to 350 nm, the absorption onset for IP-S and IP-L occurs further

Optical Materials EXPRESS

into the UV spectral range. Both IP-L and IP-S exhibit strong absorption bands at 210 nm, suggesting a much wider usable transparent window as compared to IP-Dip. In contrast to IP-Dip, the absorption onset for IP-S and IP-L is very abrupt. IP-Dip exhibits a very broad absorption onset and in addition a noticeable absorption band at approximately 230 nm. Only for IP-S a small absorption band is found inside the transparent window at approximately 358 nm. However, this band is relatively weak and may not impair the transmission of thin optical components.

4. Conclusion

The complex dielectric functions of two-photon polymerized IP-Dip, IP-L, and IP-S have been accurately determined using Mueller matrix spectroscopic ellipsometry in the range from 210 nm to 1500 nm. Parameterized dielectric function models composed of oscillators with mixed broadening including Gaussian, Lorentz, and Tauc-Lorentz broadened line shapes are used to accurately represent the optical response of the investigated polymers. In addition to enabling convenient numerical access to the complex dielectric responses of the investigated polymers, the use of parameterized dielectric functions reported here prevents instrument noise from becoming part of the established optical properties. This is a significant advantage compared to so-called point-by-point extraction techniques. The use of oscillators with mixed broadenings further enables the description of spectral ranges with measurable absorption. A good agreement of the refractive index in the transparent region is found between the results obtained here compared with literature values reported for two-photon polymerized IP-Dip in the spectral range from 400 nm to 1500 nm [24].

As expected, all investigated polymers show strong absorption bands in the UV spectral region, however, substantial differences are observed among the individual investigated polymers. While IP-Dip starts to absorb at approximately 308 nm, the transparent window of IP-L and IP-S extends to approximately 230 nm in the UV spectral range if a small absorption peak observed in IP-S at approximately 358 nm is neglected in this comparison. The location, strength, and broadening of the observed absorption bands in the UV spectral region are reported here. Comparing the refractive index of the polymers in the transparent window from 400 to 1500 nm, it can be observed that IP-S has the lowest index while IP-Dip has the highest one. Taking refractive index at wavelength of 1500 nm as an example, the values for index n are 1.526±0.008, 1.492±0.007, and 1.483±0.003 for IP-Dip, IP-L, and IP-S, respectively. In addition to providing accurate complex refractive index data, the difference between the refractive index observed for single- and two-photon polymerized IP-Dip is confirmed [24]. As suggested by S. Dottermusch *et al.* this index difference could be utilized to fabricate waveguides where the core is synthesized by single-photon polymerization while the cladding is cured using two-photon polymerization [24]. A similar refractive index difference is found for single- and two-photon polymerized IP-L and IP-S, wherein the refractive indices of the single-photon polymerized materials are reported by T. Gissibl *et al.* [22]. Therefore, optical element designs that rely on the refractive index differences of adjacent polymers could also utilize IP-L and IP-S, substantially extending the accessible range of critical dimensions for such approaches.

Our parameterized model dielectric functions for three of the most widely used polymers, which are compatible with three dimensional direct laser writing using two-photon polymerization, now provide accurate complex refractive index values for the ultraviolet to the near-infrared spectral range. Access to accurate complex refractive index data is crucial for the design and development of optical materials and components fabricated using two-photon polymerization which is receiving substantial research interest. While the results reported here are restricted to three polymers compatible with the used two-photon polymerization system, the developed mixed oscillator dielectric function model is expected to provide a flexible analysis approach, which could be also applied to other photopolymers compatible with two-photon polymerization.

Optical Materials EXPRESS

Funding

National Science Foundation within the I/UCRC center for Metamaterials (1624572); Swedish Agency for Innovation System (2014-04712); National Science Foundation.

References

1. M. Deubel, G. Von Freymann, M. Wegener, S. Pereira, K. Busch, and C. M. Soukoulis, "Direct laser writing of three-dimensional photonic-crystal templates for telecommunications," Nat. Mater. **3**(7), 444–447 (2004).
2. M. Deubel, M. Wegener, A. Kaso, and S. John, "Direct laser writing and characterization of "slanted pore" photonic crystals," Appl. Phys. Lett. **85**(11), 1895–1897 (2004).
3. M. Nawrot, Ł. Zinkiewicz, B. Włodarczyk, and P. Wasylczyk, "Transmission phase gratings fabricated with direct laser writing as color filters in the visible," Opt. Express **21**(26), 31919–31924 (2013).
4. P.-I. Dietrich, M. Blaicher, I. Reuter, M. Billah, T. Hoose, A. Hofmann, C. Caer, R. Dangel, B. Offrein, U. Troppenz, M. Moehrle, W. Freude, and C. Koos, "In situ 3D nanoprinting of free-form coupling elements for hybrid photonic integration," Nat. Photonics **12**(4), 241–247 (2018).
5. A. E. Goodling, S. Nagelberg, B. Kaehr, C. H. Meredith, S. I. Cheon, A. P. Saunders, M. Kolle, and L. D. Zarzar, "Colouration by total internal reflection and interference at microscale concave interfaces," Nature **566**(7745), 523–527 (2019).
6. Y. Li, H. Zhao, S.-F. Feng, J.-S. Ye, X.-K. Wang, W.-F. Sun, P. Han, and Y. Zhang, "New design model for high efficiency cylindrical diffractive microlenses," Sci. Rep. **7**(1), 16334 (2017).
7. T. P. Xiao, O. S. Cifci, S. Bhargava, H. Chen, T. Gissibl, W. Zhou, H. Giessen, K. C. Toussaint Jr, E. Yablonovitch, and P. V. Braun, "Diffractive spectral-splitting optical element designed by adjoint-based electromagnetic optimization and fabricated by femtosecond 3D direct laser writing," ACS Photonics **3**(5), 886–894 (2016).
8. Ł. Zinkiewicz, J. Haberko, and P. Wasylczyk, "Highly asymmetric near infrared light transmission in an all-dielectric grating-on-mirror photonic structure," Opt. Express **23**(4), 4206–4211 (2015).
9. I. Sakellari, X. Yin, M. L. Nesterov, K. Terzaki, A. Xomalis, and M. Farsari, "3D chiral plasmonic metamaterials fabricated by direct laser writing: The twisted omega particle," Adv. Opt. Mater. **5**(16), 1700200 (2017).
10. J. Moughames, S. Jradi, T. Chan, S. Akil, Y. Battie, A. E. Naciri, Z. Herro, S. Guenneau, S. Enoch, L. Joly, J. Cousin, and A. Bruyant, "Wavelength-scale light concentrator made by direct 3D laser writing of polymer metamaterials," Sci. Rep. **6**(1), 33627 (2016).
11. V. Caligiuri, R. Dhama, K. Sreekanth, G. Strangi, and A. De Luca, "Dielectric singularity in hyperbolic metamaterials: the inversion point of coexisting anisotropies," Sci. Rep. **6**(1), 20002 (2016).
12. B. Wang, Z. Xie, S. Feng, B. Zhang, and Y. Zhang, "Ultrahigh Q-factor and figure of merit fano metamaterial based on dark ring magnetic mode," Opt. Commun. **335**, 60–64 (2015).
13. T. Gissibl, S. Thiele, A. Herkommer, and H. Giessen, "Two-photon direct laser writing of ultracompact multi-lens objectives," Nat. Photonics **10**(8), 554–560 (2016).
14. M. Schmid, S. Thiele, A. Herkommer, and H. Giessen, "Three-dimensional direct laser written achromatic axicons and multi-component microlenses," Opt. Lett. **43**(23), 5837–5840 (2018).
15. M. Schumann, H. Bűckmann, N. Gruhler, M. Wegener, and W. Pernice, "Hybrid 2D-3D optical devices for integrated optics by direct laser writing," Light Sci. Appl. **3**, e175 (2014).
16. Y. Li, D. Fullager, S. Park, D. Childers, R. Fesperman, G. Boreman, and T. Hofmann, "High-contrast infrared polymer photonic crystals fabricated by direct laser writing," Opt. Lett. **43**(19), 4711–4714 (2018).
17. C. Marichy, N. Muller, L. S. Froufe-Pérez, and F. Scheffold, "High-quality photonic crystals with a nearly complete band gap obtained by direct inversion of woodpile templates with titanium dioxide," Sci. Rep. **6**(1), 21818 (2016).
18. M. Kowalczyk, J. Haberko, and P. Wasylczyk, "Microstructured gradient-index antireflective coating fabricated on a fiber tip with direct laser writing," Opt. Express **22**(10), 12545–12550 (2014).
19. Y. Li, D. Fullager, E. Angelbello, D. Childers, G. Boreman, and T. Hofmann, "Broadband near-infrared antireflection coatings fabricated by three-dimensional direct laser writing," Opt. Lett. **43**(2), 239–242 (2018).
20. X. Xiong, S.-C. Jiang, Y.-H. Hu, R.-W. Peng, and M. Wang, "Structured metal film as a perfect absorber," Adv. Mater. **25**(29), 3994–4000 (2013).
21. B. Jose, R. K. Vijayaraghavan, L. Kent, S. O'Toole, J. O'Leary, and R. J. Forster, "Tunable metallic nanostructures using 3D printed nanosphere templates," Electrochem. Commun. **98**, 106–109 (2019).
22. T. Gissibl, S. Wagner, J. Sykora, M. Schmid, and H. Giessen, "Refractive index measurements of photo-resists for three-dimensional direct laser writing," Opt. Mater. Express **7**(7), 2293–2298 (2017).
23. D. B. Fullager, G. D. Boreman, and T. Hofmann, "Infrared dielectric response of Nanoscribe IP-Dip and IP-l monomers after polymerization from 250 cm^{-1} to 6000 cm^{-1}," Opt. Mater. Express **7**(3), 888–894 (2017).
24. S. Dottermusch, D. Busko, M. Langenhorst, U. W. Paetzold, and B. S. Richards, "Exposure-dependent refractive index of nanoscribe IP-Dip photoresist layers," Opt. Lett. **44**(1), 29–32 (2019).
25. I. Faniayeu and V. Mizeikis, "Realization of a helix-based perfect absorber for ir spectral range using the direct laser write technique," Opt. Mater. Express **7**(5), 1453–1462 (2017).
26. X. Xiong, Z.-H. Xue, C. Meng, S.-C. Jiang, Y.-H. Hu, R.-W. Peng, and M. Wang, "Polarization-dependent perfect absorbers/reflectors based on a three-dimensional metamaterial," Phys. Rev. B **88**(11), 115105 (2013).

Optical Materials EXPRESS

27. J. S. Oakdale, R. F. Smith, J.-B. Forien, W. L. Smith, S. J. Ali, L. B. Bayu Aji, T. M. Willey, J. Ye, A. W. van Buuren, M. A. Worthington, S. T. Prisbrey, H. S. Park, P. A. Amendt, T. F. Baumann, and J. Biener,, "Direct laser writing of low-density interdigitated foams for plasma drive shaping," Adv. Funct. Mater. **27**(43), 1702425 (2017).
28. H. Fujiwara, *Spectroscopic Ellipsometry Principles and Applications* (John Wiley & Sons Inc., 2007).
29. C. Herzinger, B. Johs, W. McGahan, J. A. Woollam, and W. Paulson, "Ellipsometric determination of optical constants for silicon and thermally grown silicon dioxide via a multi-sample, multi-wavelength, multi-angle investigation," J. Appl. Phys. **83**(6), 3323–3336 (1998).
30. The measured experimental values for all off-diagonal Mueller matrix elements are 0±0.01, as would be expected for an isotropic sample response. Therefore, only the non-trivial on-diagonal Mueller matrix elements are reported here for brevity.
31. R. Synowicki and T. E. Tiwald, "Optical properties of bulk c-ZrO_2, c-MgO and a-As_2S_3 determined by variable angle spectroscopic ellipsometry," Thin Solid Films **455-456**, 248–255 (2004).
32. G. Jellison Jr and F. Modine, "Parameterization of the optical functions of amorphous materials in the interband region," Appl. Phys. Lett. **69**(3), 371–373 (1996).
33. J. G. E. Jellison and F. A. Modine, "Erratum: "Parameterization of the optical functions of amorphous materials in the interband region" [Appl. Phys. Lett. **69**, 371 (1996)]," Appl. Phys. Lett. **69**(14), 2137 (1996).